

# EEG-SEEGRAPH: INTERPRETING FUNCTIONAL CONNECTIVITY DISRUPTIONS IN DEMENTIAS VIA SPARSE-EXPLANATORY DYNAMIC EEG-GRAPH LEARNING

Fengcheng Wu<sup>1</sup>, Zhenxi Song<sup>1\*</sup>, Guoyang Xu<sup>1</sup>, Kaisong Hu<sup>1</sup>, Zirui Wang<sup>1</sup>, Yi Guo<sup>2</sup> and Zhiguo Zhang<sup>1</sup>

<sup>1</sup>Harbin Institute of Technology, Shenzhen, China

<sup>2</sup>Institute of Neurological Diseases, Shenzhen Bay Laboratory, Shenzhen, China

## ABSTRACT

Robust and interpretable dementia diagnosis from noisy, non-stationary electroencephalography (EEG) is clinically essential yet remains challenging. To this end, we propose *SeeGraph*, a *Sparse-Explanatory dynamic EEG-graph* network that models time-evolving functional connectivity and employs a node-guided sparse edge mask to reveal the connections that drive the diagnostic decision, while remaining robust to noise and cross-site variability. *SeeGraph* comprises four components: 1) a dual-trajectory temporal encoder that models dynamic EEG with two streams, with node signals capturing regional oscillations and edge signals capturing interregional coupling; 2) a topology-aware positional encoder that derives graph-spectral Laplacian coordinates from the fused connectivity and augments the node embeddings; 3) a node-guided sparse explanatory edge mask that gates the connectivity into a compact subgraph; and 4) a gated graph predictor that operates on the sparsified graph. The framework is trained with cross-entropy together with a sparsity regularizer on the mask, yielding noise-robust and interpretable diagnoses. The effectiveness of *SeeGraph* is validated on public and in-house EEG cohorts, including patients with neurodegenerative dementias and healthy controls, under both raw and noise-perturbed conditions. Its sparse, node-guided explanations highlight disease-relevant connections and align with established clinical findings on functional connectivity alterations, thereby offering transparent cues for neurological evaluation.

**Index Terms**— EEG, Graph neural networks, Explainable AI, Dynamic functional connectivity, Dementia

## 1. INTRODUCTION

Electroencephalography (EEG) offers practical utility for screening and monitoring in neurodegenerative dementias such as Alzheimer’s disease (AD) and frontotemporal dementia (FTD) [1] because it is low-cost, non-invasive, and offers high temporal resolution [2]. Identifying dementia related EEG patterns requires models that can operate on high-dimensional, noisy, and non-stationary signals. It is also valuable that such models generalize across sites[3] and yield insights that help interpret brain functional disruptions[4].

Earlier machine learning approaches relied on handcrafted spectral features or shallow classifiers, which are limited in capturing complex spatio-temporal dependencies[5]. Subsequent deep learning models, such as convolutional and recurrent networks, improved representation capacity yet still treated channels as grids

or sequences and thus lacked explicit modeling of brain network topology. More recent graph-based methods began to encode inter-regional relationships, but many adopt static or simplified formulations that underutilize temporal evolution[6][7]. Since pathological information is frequently embedded in the temporal evolution of network patterns rather than fixed states, existing methods struggle to capture dynamic cross-regional interactions, which undermines generalization and robustness[8, 9, 10].

At the same time, many models operate as black boxes, making their decision processes difficult to trace [11, 12]. They offer limited insight into the dynamics of functional connectivity and therefore fall short of clinical requirements for transparency and trustworthiness [13]. Post hoc explanation methods are often unstable or fail to faithfully reflect the model’s reasoning [14, 15]. These limitations highlight the need for inherently interpretable spatio-temporal graph models that provide reliable, clinically meaningful explanations while maintaining strong predictive performance. Robustness to site variability and acquisition noise also remains insufficient, leaving a gap for approaches that are both reliable and clinically interpretable[16].

Motivated by dementia pathophysiology that involves disrupted coordinated oscillations and interregional coupling[17], we propose a sparse-explanatory dynamic EEG-graph network, *SeeGraph*, that jointly covers two complementary feature domains: node-level regional oscillatory activity and edge-level amplitude-based interregional coupling. The model forms time-varying brain graphs, learns compact explanatory subnetworks while performing diagnosis, and is designed to improve interpretability and stability under noise and cross-site variability.

The main contributions of this work are:

- We introduce *SeeGraph*, an intrinsically explainable dynamic EEG-graph network that models time-varying brain networks for dementia diagnosis while localizing connectivity disruptions.
- *Quantitatively*, across a public cohort and an in-house clinical cohort, *SeeGraph* achieves *state-of-the-art* accuracy under both raw and noise-perturbed EEG, demonstrating cross-site robustness.
- *Qualitatively*, *SeeGraph* yields sparse, node-guided edge-level explanations that identify disease-relevant functional connectivity consistent with clinical evidence.

## 2. METHOD

The overall architecture of *SeeGraph*, an intrinsically explainable dynamic EEG-graph network, is illustrated in Fig. 1. First, the **dual-trajectory temporal encoder** introduces two feature domains that together cover regional oscillatory activity and interregional coupling. Node trajectories carry frequency domain spectra obtained

\*Corresponding author: Zhenxi Song (songzhenxi@hit.edu.cn). This work was supported by the National Natural Science Foundation of China (Grant No. 62306089) and the Shenzhen Science and Technology Program (Grant Nos. RCBS20231211090800003 and ZDSYS20230626091203008).

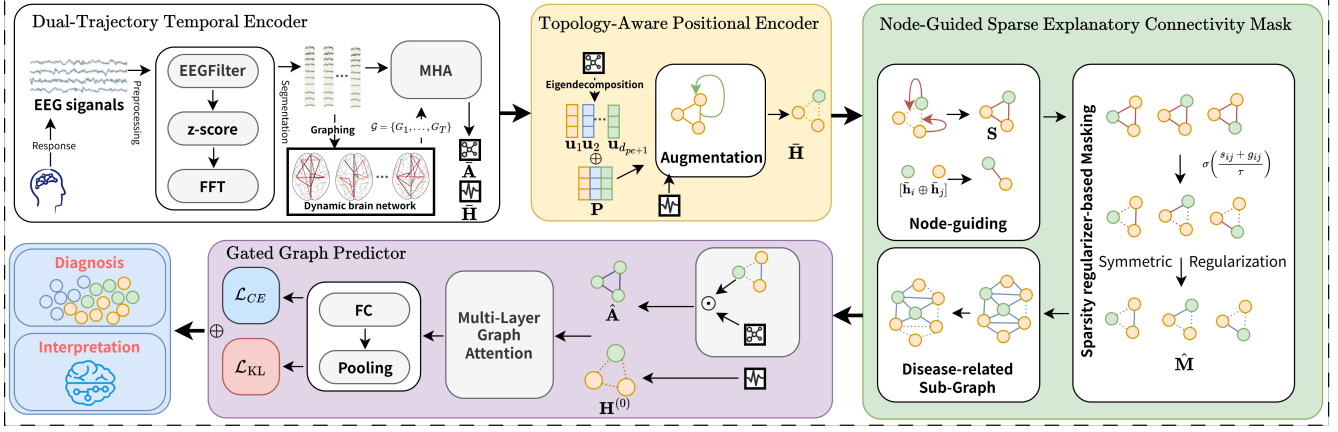


**Fig. 1.** Architecture of *SeeGraph*: dynamic EEG graphs are constructed, node and connectivity trajectories are temporally encoded, Laplacian positional encodings augment node embeddings, and a node-guided sparse mask yields an explanatory subgraph for a gated graph predictor. The objective combines diagnosis cross-entropy with a sparsity regularizer on the edge mask to learn compact, interpretable connectivity.

by FFT, while edge trajectories carry Pearson correlation computed from amplitude time series; the two streams share parameters in the dual-trajectory temporal encoder to improve data efficiency and robustness under noisy, limited clinical EEG. Second, the **topology-aware positional encoder** derives graph-spectral Laplacian coordinates from the fused edge connectivity and appends them to the node embeddings, injecting task-relevant topological context into the node domain. Third, the **node-guided sparse explanatory edge mask** conditions sparsification on pairwise node embeddings instead of raw edge weights, which avoids circular dependence on the connectivity being gated, prevents mask degeneration, and yields faithful, compact explanatory subgraphs. Fourth, the **gated graph predictor** runs graph attention on the sparsified connectivity and aggregates node representations into a graph-level embedding for diagnosis. The training objective couples cross-entropy that pulls the learned edge mask toward a low retention Bernoulli prior, implementing an information bottleneck style constraint.

## 2.1. Dual-Trajectory Temporal Encoder

As illustrated in Fig. 1, we z-score each channel and segment the  $N$ -channel EEG into  $T$  windows to form a dynamic graph sequence  $\mathcal{G} = \{G_t\}_{t=1}^T$ . Each graph  $G_t = (V, E_t, \mathbf{X}_t, \mathbf{A}_t)$  is defined so that  $V$  indexes the  $N$  EEG channels (node  $v_i$  corresponds to one channel),  $E_t$  collects the functional couplings in window  $t$ ,  $\mathbf{X}_t \in \mathbb{R}^{N \times d}$  stacks node features with row  $i$  given by  $\mathbf{x}_{i,t} \in \mathbb{R}^d$  encoding the activity of channel  $i$  at time  $t$ , and  $\mathbf{A}_t \in \mathbb{R}^{N \times N}$  is the adjacency whose entry  $a_{ij,t}$  quantifies the functional strength between  $v_i$  and  $v_j$  at time  $t$ . Unlike static methods with a fixed adjacency, we construct  $\mathbf{A}_t$  for each time window to preserve brain network dynamics.

The dual-stream temporal encoder introduces two complementary feature domains that jointly capture regional oscillatory activity and inter-regional coupling. Specifically, the continuous EEG signal is segmented into short, overlapping time windows. For each window  $t$ , we extract two types of features:

- **Node Trajectory:** for each channel  $i$  and time window  $t$ , we apply the Fast Fourier Transform (FFT) to the windowed signal to obtain a spectral vector  $\mathbf{x}_{i,t} \in \mathbb{R}^d$ . Stacking these vectors over time yields the node trajectory  $\mathbf{X}_i = [\mathbf{x}_{i,1}; \dots; \mathbf{x}_{i,T}] \in \mathbb{R}^{T \times d}$ ,

which summarizes the oscillatory activity of channel  $i$  across windows. Stacking  $\mathbf{X}_i$  across channels produces the tensor  $\mathbf{X}_{1:T} \in \mathbb{R}^{T \times N \times d}$  that collects all node tokens for the  $T$  windows.

- **Edge Trajectory:** Within each window  $t$ , we compute the absolute Pearson correlation between the amplitude time series of each pair of channels  $(i, j)$ , producing a weighted, symmetric adjacency matrix  $\mathbf{A}_t \in \mathbb{R}^{N \times N}$  with entries  $a_{ij,t}$  and zero diagonal. Stacking  $\{\mathbf{A}_t\}_{t=1}^T$  over time yields the edge trajectory tensor  $\mathbf{A}_{1:T} \in \mathbb{R}^{T \times N \times N}$ . For a specific pair  $(i, j)$ , the temporal trajectory  $\mathbf{a}_{ij,1:T} = [a_{ij,1}, \dots, a_{ij,T}]^T \in \mathbb{R}^T$  represents the evolution of interregional coupling across windows. We adopt absolute Pearson correlation for its parameter-free formulation and robustness under short-window and noisy EEG conditions.

After processing all  $T$  time windows, we construct a sequence of dynamic graphs  $\mathcal{G} = \{G_t\}_{t=1}^T$ , whose topology evolves. We then apply multi-head self-attention (MHA)[18] along the temporal axis independently to each node trajectory and each connectivity trajectory, capturing long-range temporal dependencies. Given an input sequence  $X = \{x_1, \dots, x_T\}$ , MHA computes weighted combinations of projected queries  $\mathbf{Q}_k$ , keys  $\mathbf{K}_k$ , and values  $\mathbf{V}_k$ , followed by an output projection  $\mathbf{W}^O$  [18]. Specifically, two feature streams share parameters within MHA s, improving data efficiency and robustness under noisy and limited clinical EEG conditions.

$$\text{MHA}(X) = \text{Concat}(\text{head}_1, \dots, \text{head}_H) \mathbf{W}^O, \quad (1)$$

$$\text{head}_k = \text{softmax}\left(\frac{\mathbf{Q}_k \mathbf{K}_k^\top}{\sqrt{d_k}}\right) \mathbf{V}_k, \quad (2)$$

The dual-trajectory temporal encoder fuses temporal dependencies into compact representations. It yields node embeddings  $\bar{\mathbf{H}} \in \mathbb{R}^{N \times D}$  that summarize each channel’s activity over time and a fused connectivity matrix  $\bar{\mathbf{A}} \in \mathbb{R}^{N \times N}$  that captures the evolution of functional coupling. We compute  $\bar{\mathbf{H}}$  by averaging the node time tokens, and we form  $\bar{\mathbf{A}}$  by taking the last time step of the edge stream, which emphasizes the most recent interregional interactions. We compute  $\bar{\mathbf{H}}$  by averaging the node time tokens, and we form  $\bar{\mathbf{A}}$  by taking the final attention-aggregated token of the edge stream, which emphasizes the most recent interregional interactions.

## 2.2. Topology-Aware Positional Encoder

This encoder derives Laplacian eigenvector coordinates from the fused adjacency and concatenates them with the node embeddings, thereby injecting topology-relevant positional cues into the node domain[19]. Given the temporally fused connectivity  $\bar{\mathbf{A}} \in \mathbb{R}^{N \times N}$ , let  $\mathbf{D} = \text{diag}(\bar{\mathbf{A}}\mathbf{1})$  be its degree matrix and define the (symmetric) normalized Laplacian.

$$\mathbf{L} = \mathbf{I} - \mathbf{D}^{-\frac{1}{2}} \bar{\mathbf{A}} \mathbf{D}^{-\frac{1}{2}}. \quad (3)$$

Taking the eigendecomposition of  $\mathbf{L}$  yields  $\mathbf{L} = \mathbf{U} \mathbf{\Lambda} \mathbf{U}^\top$ , where  $\mathbf{U} = [\mathbf{u}_1, \dots, \mathbf{u}_N]$  is the eigenvector matrix with columns  $\mathbf{u}_i \in \mathbb{R}^N$ , and  $\mathbf{\Lambda} = \text{diag}(\lambda_1, \dots, \lambda_N)$  are the eigenvalues in ascending order. The Laplacian positional encodings  $\mathbf{P}$  are then constructed by stacking the  $d_{\text{pe}}$  eigenvectors from  $\mathbf{U}$  that correspond to the smallest nonzero eigenvalues:

$$\mathbf{P} = [\mathbf{u}_2, \dots, \mathbf{u}_{d_{\text{pe}}+1}] \in \mathbb{R}^{N \times d_{\text{pe}}}. \quad (4)$$

We then augment graph connectivity embeddings via concatenation:

$$\bar{\mathbf{H}} \leftarrow [\bar{\mathbf{H}} \parallel \mathbf{P}] \in \mathbb{R}^{N \times (D+d_{\text{pe}})}. \quad (5)$$

By embedding both local activity and global structure, the model gains a more holistic understanding of brain dynamics.

## 2.3. Node-Guided Sparse Explanatory Connectivity Mask

This module is designed to identify a sparse and informative network by learning a stochastic connectivity mask[20]. It operates in an *connectivity-wise* manner, where the importance of each potential connectivity is computed directly from the embeddings of its endpoint nodes.

Specifically, for each potential connectivity  $(v_i, v_j)$ , the Extractor takes the corresponding time-aggregated node embeddings  $\bar{\mathbf{h}}_i$  and  $\bar{\mathbf{h}}_j$  from the previous stage. These two embeddings are concatenated to form a feature vector  $[\bar{\mathbf{h}}_i \oplus \bar{\mathbf{h}}_j]$  that uniquely represents the connectivity. This vector is then passed through a shared Multi-Layer Perceptron (MLP) to produce a single logit  $s_{ij}$  quantifying the connectivity’s relevance. Repeating this for all pairs yields the full *connectivity-logit matrix*  $\mathbf{S} \in \mathbb{R}^{N \times N}$ .

From these logits, a differentiable *binary-concrete* (Gumbel-Sigmoid) mask  $\mathbf{M} \in (0, 1)^{N \times N}$  is sampled:

$$m_{ij} = \sigma\left(\frac{s_{ij} + g_{ij}}{\tau}\right), \quad g_{ij} \sim \text{Logistic}(0, 1), \quad (6)$$

where  $\tau > 0$  is a temperature parameter that is annealed during training. To ensure the resulting network is undirected, the mask is made symmetric and its diagonal is zeroed out:

$$\tilde{\mathbf{M}} = \text{SymmZeroDiag}(\mathbf{M}) = \frac{\mathbf{M} + \mathbf{M}^\top}{2} - \text{diag}(\text{diag}(\mathbf{M})). \quad (7)$$

To encourage sparsity and prevent the model from selecting all connectivity, a KL divergence penalty aligns the mask distribution with a Bernoulli prior[21, 22] of mean  $r$ :

$$\mathcal{L}_{\text{KL}} = \frac{1}{N(N-1)} \sum_{i \neq j} \left[ m_{ij} \log \frac{m_{ij}}{r + \epsilon} + (1 - m_{ij}) \log \frac{1 - m_{ij}}{1 - r + \epsilon} \right], \quad (8)$$

where  $\epsilon$  ensures numerical stability. Sparsification is performed based on pairwise node embeddings rather than raw edge weights, which avoids circular dependence on the connectivity being gated, prevents mask degeneration, and yields reliable and compact explanatory brain network.

## 2.4. Gated Graph Predictor

To form the input graph structure for classification, we construct a gated adjacency matrix by applying the learned explanatory mask to the temporally fused connectivity:

$$\hat{\mathbf{A}} = \tilde{\mathbf{M}} \odot \bar{\mathbf{A}}, \quad (9)$$

where  $\bar{\mathbf{A}} \in \mathbb{R}^{N \times N}$  is the dynamic connectivity matrix aggregated over time. This gating mechanism selectively retains the most relevant connections, and The resulting  $\hat{\mathbf{A}}$  is used in subsequent graph learning steps to guide the learning process in the network for diagnosis.

Let  $\mathbf{H}^{(0)} = [\bar{\mathbf{H}} \parallel \mathbf{P}] \in \mathbb{R}^{N \times (D+d_{\text{pe}})}$  be the initial node-feature matrix. A multi-layer GAT[23] runs on  $\hat{\mathbf{A}}$ , updating rows of  $\mathbf{H}^{(l)}$  as

$$\mathbf{H}_i^{(l+1)} = \sigma \left( \sum_{j \in \mathcal{N}_{\hat{\mathbf{A}}}(i)} \hat{a}_{ij} \alpha_{ij}^{(l)} \mathbf{W}^{(l)} \mathbf{H}_j^{(l)} \right), \quad (10)$$

where  $\hat{a}_{ij}$  is the  $(i, j)$ -entry of the explanatory adjacency  $\hat{\mathbf{A}}$ ,  $\alpha_{ij}^{(l)}$  are GAT attention coefficients, and  $\mathbf{W}^{(l)}$  are learnable weights. After graph-level pooling, we obtain a graph representation for classification and train the model by minimizing the objective:

$$\mathcal{L} = \mathcal{L}_{\text{CE}} + \lambda_{\text{KL}} \mathcal{L}_{\text{KL}}, \quad (11)$$

The training objective combines cross-entropy loss with a term that pulls the learned edge mask toward a low retention Bernoulli prior, thereby implementing an information bottleneck-style constraint. Here,  $\lambda_{\text{KL}}$  is a hyperparameter that balances the trade-off between predictive accuracy and the sparsity of the explanation.

This mechanism distills the dynamic brain network into a sparse, clinically meaningful subgraph that makes explicit which connections drive the diagnosis, thereby enhancing transparency and robustness by filtering spurious relations.

## 3. EXPERIMENTS AND RESULTS

### 3.1. Experimental Setup

**Datasets.** We used two EEG datasets. (i) AHEPA: a public resting-state EEG cohort collected at AHEPA University Hospital [29]. It includes 88 participants: 36 with AD, 23 with FTD, and 29 healthy controls (HC). Recordings were acquired in the eyes-closed condition with a 19-channel 10–20 system at 500 Hz. We treat this as a three-class classification task and report macro-averaged metrics across classes. (ii) SZPH: a clinical cohort from Shenzhen People’s Hospital comprising EEG from patients with AD and HC. A total of 50 participants remained (30 AD, 20 HC) after diagnostic screening. Recordings used a 64-channel 10–20 system.

**Implementation details.** We implemented *SeeGraph* in PyTorch and ran all experiments on an NVIDIA RTX 3090 GPU. Evaluation was conducted on the in-house SZPH cohort and the public AHEPA cohort. Experiments were conducted independently per dataset. Differences in sampling rates and channel counts were handled via consistent band-limiting and spectral feature extraction.

### 3.2. Experimental Results

To ensure fair comparison in our subject-independent clinical setting, we focus on representative dynamic GNN and temporal baselines rather than externally pretrained EEG foundation models. Baselines include: dynamic GNNs such as EvolveGCN-O [26],

**Table 1.** Performance comparison on the SZPH and AHEPA datasets under normal and noisy conditions

Method	SZPH Dataset (China)						AHEPA Dataset (Greece)					
	Raw (no added noise)			Noisy			Raw (no added noise)			Noisy		
	ACC	AUROC	F1	ACC	AUROC	F1	ACC	AUROC	F1	ACC	AUROC	F1
BIOT[24]	0.765	0.820	0.761	0.621	0.767	0.607	0.812	0.937	0.798	0.733	0.786	0.712
DCRNN[25]	0.760	0.819	0.779	0.661	0.740	0.737	0.738	0.819	0.719	0.651	0.734	0.657
EGCN[26]	0.734	0.726	0.718	0.645	0.643	0.660	0.648	0.769	0.614	0.602	0.736	0.522
CNN-LSTM	0.770	0.804	0.772	0.723	0.731	0.695	0.635	0.752	0.556	0.592	0.631	0.542
STGCN[27]	0.772	0.831	0.761	0.743	0.785	0.717	0.645	0.778	0.628	0.623	0.758	0.603
MATT[28]	0.613	0.653	0.630	0.583	0.626	0.571	0.669	0.729	0.627	0.635	0.701	0.589
<b>SeeGraph</b>	<b>0.874</b>	<b>0.951</b>	<b>0.875</b>	<b>0.848</b>	<b>0.926</b>	<b>0.849</b>	<b>0.841</b>	<b>0.953</b>	<b>0.834</b>	<b>0.827</b>	<b>0.937</b>	<b>0.822</b>

**Table 2.** Diagnostic utility of EEG frequency bands for dementia diagnosis across two cohorts

Bands	SZPH Dataset (China)						AHEPA dataset (Greece)					
	Raw (no added noise)			Noisy			Raw (no added noise)			Noisy		
	ACC	AUROC	F1	ACC	AUROC	F1	ACC	AUROC	F1	ACC	AUROC	F1
$\delta$ (Delta)	0.693	0.795	0.716	0.663	0.765	0.664	NAN	NAN	NAN	NAN	NAN	NAN
$\theta$ (Theta)	0.702	0.867	0.621	<b>0.815</b>	<b>0.830</b>	<b>0.804</b>	0.739	0.897	0.719	0.725	0.876	0.710
$\alpha$ (Alpha)	0.792	0.817	0.773	0.729	0.816	0.745	<b>0.881</b>	<b>0.969</b>	<b>0.876</b>	<b>0.832</b>	<b>0.937</b>	<b>0.851</b>
$\beta$ (Beta)	<b>0.828</b>	<b>0.887</b>	<b>0.818</b>	0.785	0.862	0.764	0.827	0.948	0.820	0.789	0.895	0.763
$\gamma$ (Gamma)	0.708	0.819	0.748	0.692	0.770	0.660	0.681	0.859	0.676	0.676	0.815	0.663

DCRNN [25], and STGCN [27], and temporal models including BIOT [24], CNN-LSTM, and MAtt [28]. All experiments use a subject-independent 80/20 train–test split at the subject level.

As shown in Table 1, **SeeGraph** achieves the best metrics on both the SZPH and AHEPA datasets, confirming the benefits of the two-stream temporal encoding and node-guided sparse edge gating. The same table reports robustness under additive Gaussian noise (zero mean, standard deviation 0.3) injected into the input signals. Under these noisy conditions, **SeeGraph** exhibits only minor performance degradation, demonstrating robustness, effective modeling of long-range temporal dependencies, and generalization across varying data quality.

**Table 3.** Ablation study of **SeeGraph**

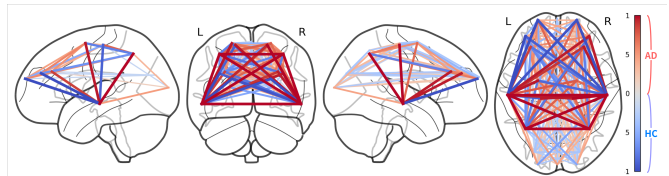
Method	SZPH			AHEPA		
	ACC	AUROC	F1	ACC	AUROC	F1
<b>SeeGraph</b>	<b>0.874</b>	<b>0.951</b>	<b>0.875</b>	<b>0.841</b>	<b>0.953</b>	<b>0.834</b>
w/o C-wise	0.855	0.938	0.862	0.823	0.904	0.805
w/o PE	0.837	0.905	0.841	0.824	0.918	0.829
w/o SR	0.770	0.864	0.761	0.812	0.937	0.798
w/o FFT	0.758	0.842	0.772	0.784	0.924	0.768

For scientific validation and clinical relevance, we conduct a band-wise analysis to quantify each EEG band’s contribution to dementia diagnosis. Results (Table 2) shows that  $\alpha$ ,  $\beta$ , and  $\delta$  carry the strongest diagnostic signal,  $\theta$  is moderate, and  $\gamma$  is comparatively weak. In the AHEPA cohort, the  $\delta$ -band is unavailable after their original preprocessing, yielding NA entries. These findings are consistent with clinical evidence of  $\alpha$  attenuation,  $\beta$  suppression, and  $\delta$  elevation in dementia, thereby reinforcing the plausibility and interpretability of the learned features.

We conducted ablation experiments to assess the contribution of each module in **SeeGraph**. As shown in Table 3, removing any single component degrades performance, indicating complementary contributions to representation learning. Removing the connectivity stream (w/o C-wise) lowers all metrics, underscoring the importance of modeling inter-channel relationships. Discarding positional encodings (w/o PE) also reduces F1, showing that topological cues aid both accuracy and interpretability. Turning off the sparsity regularizer on the edge mask (w/o SR, i.e.,  $\lambda_{KL} = 0$ ) reduces AUROC and produces denser, less faithful explanations. Omitting frequency-domain features (w/o FFT) yields a marked drop, confirming the

utility of spectral information for brain dynamics. Collectively, these results support the indispensability of each module in **SeeGraph**.

To illustrate the model’s explainability, we visualize disease-relevant brain connectivity on the SZPH cohort, showing how **SeeGraph** captures and integrates temporal dependencies and interregional functional coupling. As shown in Fig. 2, disease-relevant edges concentrate in fronto-temporal circuitry. AD exhibits temporal-lobe-centered clustering, whereas HC retains more inter-hemispheric bridges and a more symmetric bilateral fronto-temporal integration.

**Fig. 2.** **SeeGraph** localizes salient fronto-temporal subnetworks via a node-guided sparse mask. AD exhibits temporal-centered ipsilateral clustering (red), while HC shows more inter-hemispheric and bilateral integration (blue); darker colors indicate higher salience.

#### 4. CONCLUSION

This paper presents **SeeGraph**, a sparse-explanatory dynamic EEG-graph network addressing the dual challenges of robustness and interpretability in dementia diagnosis. By modeling time-varying brain networks, **SeeGraph** jointly captures regional oscillations and interregional coupling, extracts clinically meaningful subnetworks through a node-guided sparse masking mechanism. The model integrates spectral and topological cues via a dual-trajectory encoder and Laplacian-based positional encoding, supporting transparent diagnostic reasoning. Experiments on a public and a clinical EEG cohort show that **SeeGraph** achieves superior performance under clean and noisy conditions. Ablation and interpretability analyses validate each component and the alignment of extracted patterns with clinical findings. **SeeGraph** thus offers a robust and explainable framework for EEG-based neurodegenerative disease analysis.

## 5. REFERENCES

- [1] L. Jia, T. Jiang, and C. Liu, "Prevalence, risk factors, and management of dementia and mild cognitive impairment in adults aged 60 years or older in China: A cross-sectional study," *The Lancet Public Health*, vol. 5, no. 12, pp. e661–e671, 2020.
- [2] D. Cai, J. Chen, and Y. Yang, "Mbrain: A multi-channel self-supervised learning framework for brain signals," in *Proceedings of the 29th ACM SIGKDD Conference on Knowledge Discovery and Data Mining*, 2023, pp. 130–141.
- [3] M. Hata, M. A. Johnson, and N. Simonian, "Accurate deep-learning model to differentiate dementia severity and diagnosis using a portable eeg device," *Scientific Reports*, vol. 15, pp. 12526, 2025.
- [4] T. Jungrungrueang, O. Phokaewvarangkul, and K. Wongkum, "Translational approach for dementia subtype classification using convolutional neural network based on eeg connectome dynamics," *Scientific Reports*, vol. 15, no. 1, pp. 17331, 2025.
- [5] Daniel Klepl, Mengying Wu, and Feng He, "Graph neural network-based EEG classification: A survey," *IEEE Transactions on Neural Systems and Rehabilitation Engineering*, vol. 32, pp. 493–503, 2024.
- [6] J. Gao, J. Liu, Y. Xu, D. Peng, and Z. Wang, "Brain age prediction using the graph neural network based on resting-state functional MRI in alzheimer's disease," *Frontiers in Neuroscience*, vol. 17, pp. 1222751, 2023.
- [7] R. Qin, Z. Song, H. Ren, Z. Pei, L. Zhu, X. Shi, Y. Guo, H. Liu, M. Zhang, and Z. Zhang, "Bnmtrans: A brain network sequence-driven manifold-based transformer for cognitive impairment detection using eeg," in *Proceedings of the IEEE International Conference on Acoustics, Speech and Signal Processing (ICASSP)*, 2024, pp. 2016–2020.
- [8] M. Graña and I. Morais-Quilez, "A review of graph neural networks for electroencephalography data analysis," *Neurocomputing*, vol. 562, pp. 126901, 2023.
- [9] S. Wu, F. Sun, and W. Zhang, "Graph neural networks in recommender systems: A survey," *ACM Computing Surveys*, vol. 55, no. 5, pp. 1–37, 2022.
- [10] M. Li, A. Micheli, and Y. G. Wang, "Guest editorial: Deep neural networks for graphs: Theory, models, algorithms, and applications," *IEEE Transactions on Neural Networks and Learning Systems*, vol. 35, no. 4, pp. 4367–4372, 2024.
- [11] X. Zhou, *Interpretable and Robust AI in Electroencephalogram Systems*, Ph.D. thesis, Nanyang Technological University, 2025.
- [12] A. Craik, Y. He, and J. L. Contreras-Vidal, "Deep learning for electroencephalogram (EEG) classification tasks: A review," *Journal of Neural Engineering*, vol. 16, no. 3, pp. 031001, 2019.
- [13] H. Yang, X. Chen, and Z. B. Chen, "Disrupted intrinsic functional brain topology in patients with major depressive disorder," *Molecular Psychiatry*, vol. 26, no. 12, pp. 7363–7371, 2021.
- [14] W. Samek, G. Montavon, and S. Lapuschkin, "Explaining deep neural networks and beyond: A review of methods and applications," *Proceedings of the IEEE*, vol. 109, no. 3, pp. 247–278, 2021.
- [15] Z. Song, R. Qin, H. Ren, Z. Liang, Y. Guo, M. Zhang, and Z. Zhang, "Eeg-macs: Manifold attention and confidence stratification for eeg-based cross-center brain disease diagnosis under unreliable annotations," in *Proceedings of the 32nd ACM International Conference on Multimedia*, Melbourne, VIC, Australia, 2024, pp. 340–349.
- [16] Z. Wang, Z. Song, Y. Guo, Y. Liu, G. Xu, M. Zhang, and Z. Zhang, "Eeg-remind: Enhancing neurodegenerative eeg decoding through self-supervised state reconstruction-primed riemannian dynamics," in *Proceedings of the IEEE International Conference on Acoustics, Speech and Signal Processing (ICASSP)*, 2025, pp. 1–5.
- [17] Z. Song, B. Deng, J. Wang, and R. Wang, "Biomarkers for Alzheimer's disease defined by a novel brain functional network measure," *IEEE Transactions on Biomedical Engineering*, vol. 66, no. 1, pp. 41–49, 2019.
- [18] A. Vaswani, N. Shazeer, and N. Parmar, "Attention is all you need," in *Advances in Neural Information Processing Systems*, 2017, vol. 30.
- [19] V. P. Dwivedi, C. K. Joshi, and A. T. Luu, "Benchmarking graph neural networks," *Journal of Machine Learning Research*, vol. 24, no. 43, pp. 1–48, 2023.
- [20] S. Miao, M. Liu, and P. Li, "Interpretable and generalizable graph learning via stochastic attention mechanism," in *Proceedings of the International Conference on Machine Learning*, 2022, pp. 15524–15543, PMLR.
- [21] E. Jang, S. Gu, and B. Poole, "Categorical reparameterization with gumbel-softmax," *arXiv preprint arXiv:1611.01144*, 2016.
- [22] N. Tishby and N. Zaslavsky, "Deep learning and the information bottleneck principle," in *2015 IEEE Information Theory Workshop (ITW)*, 2015, pp. 1–5, IEEE.
- [23] P. Veličković, G. Cucurull, and A. Casanova, "Graph attention networks," *arXiv preprint arXiv:1710.10903*, 2017.
- [24] C. Yang, M. Westover, and J. Sun, "Biot: Biosignal transformer for cross-data learning in the wild," in *Advances in Neural Information Processing Systems*, 2023, vol. 36, pp. 78240–78260.
- [25] S. Tang, J. A. Dunnmon, and K. Saab, "Self-supervised graph neural networks for improved electroencephalographic seizure analysis," *arXiv preprint arXiv:2104.08336*, 2021.
- [26] A. Pareja, G. Domeniconi, and J. Chen, "Evolvegcn: Evolving graph convolutional networks for dynamic graphs," in *Proceedings of the AAAI Conference on Artificial Intelligence*, 2020, vol. 34, pp. 5363–5370.
- [27] Z. Shao, Z. Zhang, and F. Wang, "Pre-training enhanced spatial-temporal graph neural network for multivariate time series forecasting," in *Proceedings of the 28th ACM SIGKDD Conference on Knowledge Discovery and Data Mining*, 2022, pp. 1567–1577.
- [28] Y. T. Pan, J. L. Chou, and C. S. Wei, "Matt: A manifold attention network for EEG decoding," in *Advances in Neural Information Processing Systems*, 2022, vol. 35, pp. 31116–31129.
- [29] A. Miltiadous, K. D. Tzamourta, and T. Afrantou, "A dataset of scalp EEG recordings of alzheimer's disease, frontotemporal dementia and healthy subjects from routine EEG," *Data*, vol. 8, no. 6, pp. 95, 2023.